In-situ Fabrication of Carbon-metal fabrics as Freestanding Electrodes for High-performance All-solid-state Energy Storage Devices

Xinhua Liu[1,+], Mengzheng Ouyang[2,+], Marcin W Orzech,[4] Yubiao Niu[4], Weiqiang Tang,[5,6] Jingyi Chen,[1] Max Naylor Marlow[1], Debashis Puhan,[5] Yan Zhao,[3] Rui Tan,[2,8] Brankin Colin[1,9], Nicholas Haworth[1,7], Shuangliang Zhao,[6] Huizhi Wang,[5] Peter Childs[1], Serena Margadonna,[4] Marnix Wagemaker,[10] Feng Pan,[3*] Nigel Brandon,[2] Chandramohan George[1*] and Billy Wu[1*]

[1]Dyson School of Design Engineering, Imperial College London, SW7 2AZ, London, UK
[2]Earth Science and Engineering, Imperial College London SW7 2AZ, London, UK
[3]School of Advanced Materials, Peking University Shenzhen Graduate School, 518055, Shenzhen, China
[4]College of Engineering, Swansea University, Swansea SA1 8PP, UK
[5]Department of Mechanical Engineering, Imperial College London SW7 2AZ, London, UK
[6]State Key Laboratory of Chemical Engineering and School of Chemical Engineering, East China University of Science and Technology, Shanghai 200237, China
[7]Department of Materials, Imperial College London SW7 2AZ, London, UK
[8]Department of Chemical Engineering, Imperial College London SW7 2AZ, London, UK
[9]Department of Chemical and Biomolecular Engineering, University of Notre Dame, 46556, Indiana, USA
[10]Department of Radiation Science and Technology, Delft University of Technology, Delft, Netherlands

Keywords

Carbon-metal fabrics, non-woven, Electrospinning, Nanofibers, Carbon, Metal-air Battery, all-solid-state

Abstract

1D carbon structures are attractive due to their mechanical, chemical and electrochemical properties. Further enhancements to these structures can be made by creating structural hierarchy, producing composites with catalytically active metal nanoparticle domains - however the synthesis of these materials can be costly and complicated. Here, through the combination of inexpensive acetylacetonate salts of Ni, Co and Fe with a solution of polyacrylonitrile (PAN) which was electrospun and subsequently heat treated, self-assembling carbon-metal fabrics (CMFs) containing unique 1D hierarchical structures can be created readily. Microscopic and spectroscopic measurements show that the CMFs form through the decomposition and exsolution of metal nanoparticle domains which then catalyse the formation of carbon nanotubes through the decomposition by-products of the PAN. These weakly bound nanoparticles form structures similar to trichomes found in plants, with a combination of base-growth, tip-growth and peapod-like structures, where the metal domain exhibits a core(graphitic)-shell(disorder)

carbon coating where the thickness is in-line with the metal-carbon binding energy. The applicability of these carbon-metal fabrics (CMFs) was demonstrated as a cathode in an all-solid-state zinc-air battery which exhibited superior performance to pure electrospun carbon fibres, in addition to enhanced mechanical flexibility due to the enhanced surface area of the hairy fibres and their metallic nanoparticle domains which acted as bifunctional catalysts to oxygen reduction and evolution. This work therefore unlocks a potentially new category of composite metal-carbon fibre based structures for energy storage applications and beyond, which can be created in a low cost manner.

Introduction

1D carbon based structures such as carbon nanotubes (CNT) and carbon nanofibres (CNF) are attractive due to their continuous nature, chemical stability and the ability to be functionalised which are advantageous in a range of applications.[1,2] However, despite their promise, they suffer from manufacturing issues due to their desired structures requiring many fabrication steps, such as functionalisation, surface conditioning and coating. Since the discovery of CNTs[3], many types of carbon structures, composites and hybrids have been developed and exploited in applications including lithium-ion (Li-ion) batteries [4,5], energy conversion and catalysis. [6,7] In particular, 1D carbon based structures[8] across different length scales built into 3D scaffolds have shown attractive performance, for example, carbon papers for proton exchange membrane fuel cells[9], CNFs for supercapacitors[10], lithium-sulphur batteries[11] and metal-air batteries[12]. Each length scale of interest offers certain advantages. Macro-scale fibres offer ease of fabrication and good electronic conductivity, submicron scale features exhibit good electrochemical performance, and nano-scale tubes provide enhanced mechanical properties. Thus, the potential of synthesising hierarchical carbon based structures that integrate the above multi-length scale characteristics into a single material is extremely attractive.

Various methods exist to synthesize these structures which includes the deposition of nano-scale catalyst particles onto substrates and subsequent growth of CNTs via processes such as chemical vapour deposition (CVD) which, whilst effective, are expensive and time consuming. On the other

hand, electrospinning is a well-developed and industrially adopted process for manufacturing carbon fibres [13,14,15]. In this process a polymer and solvent, such as polyacrylonitrile (PAN) in N,N-dimethylformamide (DMF), is extruded through a nozzle and spun into micron to nano sized fibres via the application of a high voltage electric field. The subsequent fibres are then pyrolysed at high temperatures to produce carbon structures. Based on this technique, carbon mats, felt and fabrics with non-woven fibres have been produced and exploited as separators and electrodes in Li-ion batteries[16,17], binderless anodes with MoS_2 for sodium ion batteries[18], cathodes for zinc-air batteries[19,20] and as supercapacitor electrodes when combined with metal-oxides.[21] Although electrospinning is capable of producing free-standing structures, most of them do not span multiple length scales and thus do not exploit the potential material properties. For example, electrospun fabrics tend to be fragile and mechanically weak and with a small surface area compared to other forms of carbon. To mitigate this, approaches such as incorporating nanoparticles to improve surface area[22,23], electro-netting with a polymer, carbon, titanium oxide[24] to improve electronic conductivity and deposition of palladium nanoparticles and consequent CNT growth to make secondary fibres [25] with catalytic functions have been developed.

Recently, an important breakthrough was achieved through a carbothermal shock synthesis route which enabled the production of multicomponent nanoparticles (high entropy alloys) on carbon nanofibers, exhibiting remarkable catalytic properties which highlighted the potential of functionalising CNFs.[26] Although some progress has been made in preparing hierarchical nanocomposites and in understanding the associated CNT and CNF growth mechanisms, current manufacturing routes are still expensive and complex. Thus, motivated by this, we present a scalable synthesis route for hierarchical CNFs with catalytically active metal nanoparticle domains through the modification of existing industrial techniques. The applicability of this material is demonstrated as a bifunctional cathode for a zinc-air battery which exhibits mechanical robustness, flexibility and stable performance with the potential to be transferred into other applications.

Drawing inspiration from trichomes, the fine bristle like micro-nano structures found in certain plants and insects, we present an architectural material that can integrate material functionalities at different

length scales (nano-micro-macro), which we term carbon metal fabrics (CMFs). By combining electrospinning and a floating catalyst pyrolysis synthesis route, we demonstrate a scalable and tractable production method for CMFs that produces hierarchical morphologies ideal for energy storage applications. These CMFs consist of micron-sized electrospun non-woven carbon fibres covered in bristles of carbon nanotubes that encase catalytically active metal nanoparticles (Fe, Ni and Co). Our structural, spectroscopic and microscopic analysis of these CMFs present new insights into the microstructural features of these carbon-metal composites, highlighting unique features conducive to development of high performance energy-storage devices as well as understanding their synthesis mechanisms. As a proof of concept, we designed and fabricated a series of all-solid-state Zn-air batteries using these CMFs. The battery performance in terms of current density, capacity and capability further underpins the benefits of these hierarchical composite nanocarbon, metal nanoparticles and carbon fibre materials as battery electrodes.

Results and Discussion

A tractable manufacturing route for non-woven CMFs has been developed by combining electrospinning and pyrolysis. The non-woven electrospun fibres, which serve as the skeleton for the CMFs, are approximately 600 nm in diameter and have lengths in the centimetre length scale. Detailed fabrication methods and procedures are provided in the supporting information. In brief, organometallic salts (acetylacetonate forms of Fe, Co or Ni) were mixed with a polymer solution of PAN in DMF. Electrodes with thicknesses of up to 500 microns were fabricated by controlling the electrospinning time. These electrospun fibres were then subjected to a stabilisation process at 290 °C in air for 2 h and a pyrolysis step at 850 °C in nitrogen (N_2), where the organometallic salts (Fe, Ni or Co) decompose at temperatures of approximately 170 °C. This gives rise to the formation of well-faceted metal nanoparticles through an exsolution mechanism, which are randomly distributed on the surface of the electrospun fibres (Fig. 1). Control experiments during heat treatment show the gradual emergence of Fe, Co and Ni nanoparticles during stabilisation and carbonisation across the fibres (Supplementary Figs. S1-S3). This carbonisation method where the catalyst precursors are introduced in the initial electrospinning solution is known as floating catalysis, meaning that catalyst particles are

self-assembled *in situ* during the heat treatment process, as opposed to other methods where catalysts are applied directly as nanoparticles at the start of the reaction or after CNF synthesis (Supplementary Table S1). As a result, the newly formed catalyst particles tend to freely diffuse and migrate to the surface of the CNF to minimise their free energy leading to the growth of secondary CNTs. Evidently, the appearance of carbon nanotubes like bristle or hairs on the primary electrospun fibres at temperatures above 600 °C is caused by the presence of catalyst particles which exhibit a combination of base growth, tip growth and peapod like CNT structures as shown in Fig. 1 and the supporting information. Most of the carbonised electrospun fibres run parallel whilst some crisscross, serving as primary scaffoldings for the CMFs, which can then be reinforced by the presence of bristle like growth of carbon nanotubes capable of interlocking the fibres when in contact (similar to Velcro). Such an arrangement further imparts the fabrics with robustness and mechanical pliability, whilst the infiltration of metal either as elongated nanoparticles or rods into the bristle like CNTs provide additional structural support. The resulting structure is a free standing CMF with mechanical flexibility, capable of being rolled and even twisted (see later).

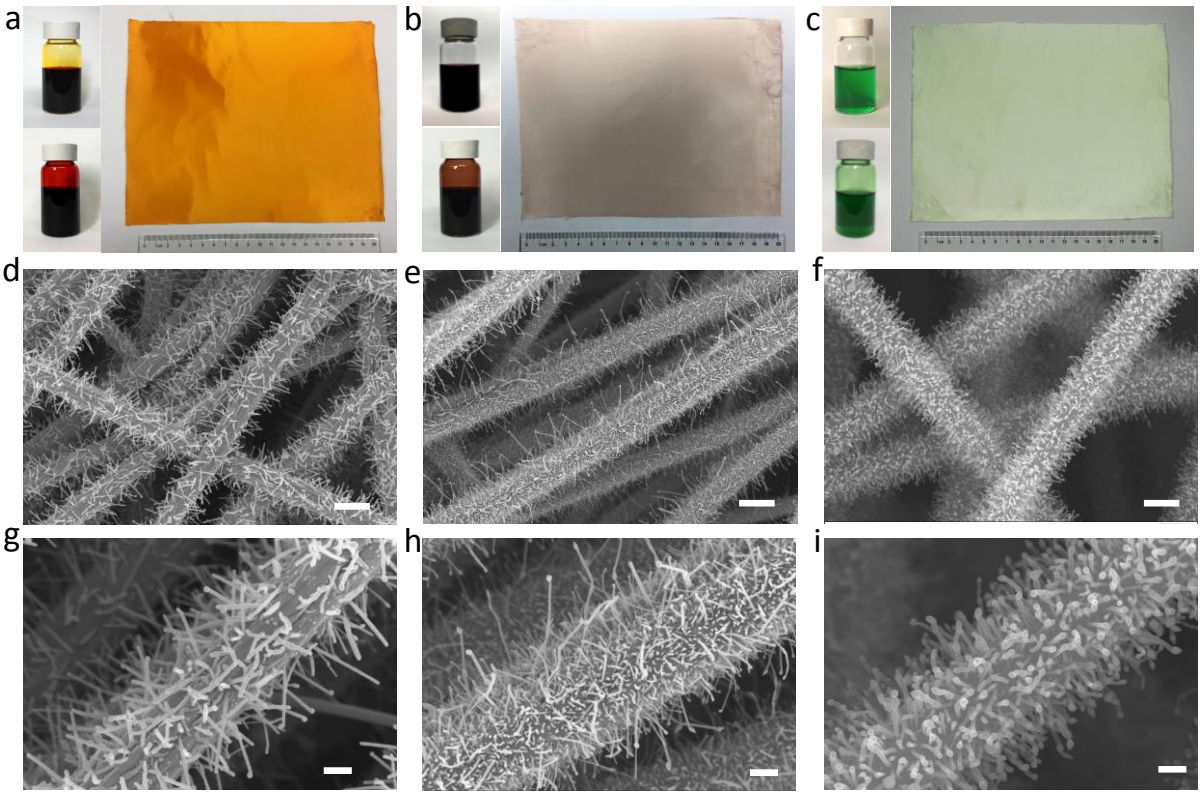

Fig. 1 | SEM images of hairy fibers. Mixed solutions in bottles: $M(acac)_X$+DMF (upper), $M(acac)_X$+DMF+PAN (lower), and their electrospun nanofiber films. a, M=Fe, x=3, $Fe(acac)_3$, b, M=Co, x=2, $Co(acac)_2$, c, M=Ni, x=2, $Ni(acac)_2$. d, g, SEM images of Fe based hairy carbon nanofiber. e, h, SEM images of Co based hairy carbon nanofiber. f, i, SEM images of Fe based hairy carbon nanofiber. (The scale bar in 1 μm for d, e, f and 200 nm for g, h, I)

Fig. 2 shows the high-angle annular dark-field- scanning transmission electron microscope (HAADF-STEM) images of all the three CMFs (Fe, Co, and Ni). In many nanotubes, metal in the form of nanorods infiltrates the CNTs, which may be the reason for the growth of peapod like structures (Supplementary Fig. S4) depending on the local kinetics and strain. For most of the Ni and Co based nanotubes, the metal nanoparticles exhibited "peapod" type structures (Supplementary Figs. S4-S5), with multiple graphitic layers, which are an intermediate growth mechanism between the typical tip and base growth modes. In most of the cases, the metal nanoparticle domains found at the tip of the tubes are covered by either thick (15 nm) or thin (3 nm) carbon shells. These regions consist of well-crystallised metal particles (~40-60 nm) which are encapsulated in graphitic/disordered carbon layers, as shown by high resolution transmission electron microscopy (HRTEM) (Fig. 2). Interestingly, the Fe-based fabrics generally have thinner carbon coatings, with these being mostly graphitic.

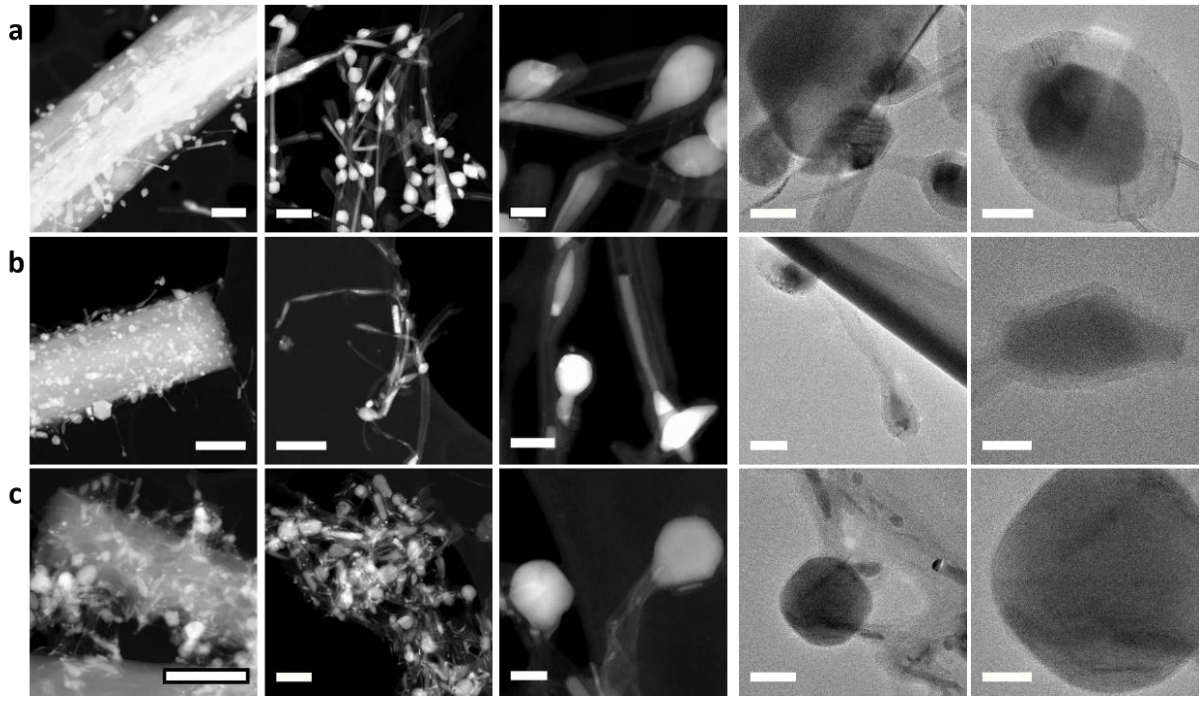

Fig. 2 | High-angle annular dark-field (HAADF-STEM) and high resolution TEM images of carbon metal fabrics (CMFs). a, Ni based CMFs. b, Co based hairy carbon nanofiber. c, Fe based CMFs. The first image in each row shows larger carbon nanofiber, while the following zoom in on the "bristles" and encapsulated metal

nanoparticles. The scale bars in each column starting from left are 400 nm, 200 nm, 50 nm, 50 nm and 20 nm respectively.

To gain insights into the chemical composition of these fabrics, Energy-dispersive X-ray spectroscopy (EDS) analysis was performed. The TEM images in Fig. 3 show a homogenous distribution of carbon in the electrospun fibres (Figs. 3a, 3c, 3e) and the presence of metals (Fe, Co or Ni) as nanoparticles from which bristle like carbon nanotube had grown. A focused-ion beam scanning electron microscope (FIBSEM) reconstruction movie is presented in the supporting information and shows the presence of metal particles both on the surface and bulk of electrospun fibres. The presence of the carbon shell around the Co and Ni domains and thin shells around the Fe nanoparticles can be distinguished from this mapping (Figs. 3b, 3d, 3e). When measuring the intensity of the carbon signals in the nanoparticle region, the intensity for the Fe based fabrics is lower than that of the Co and Ni, further confirming the thinner carbon coating.

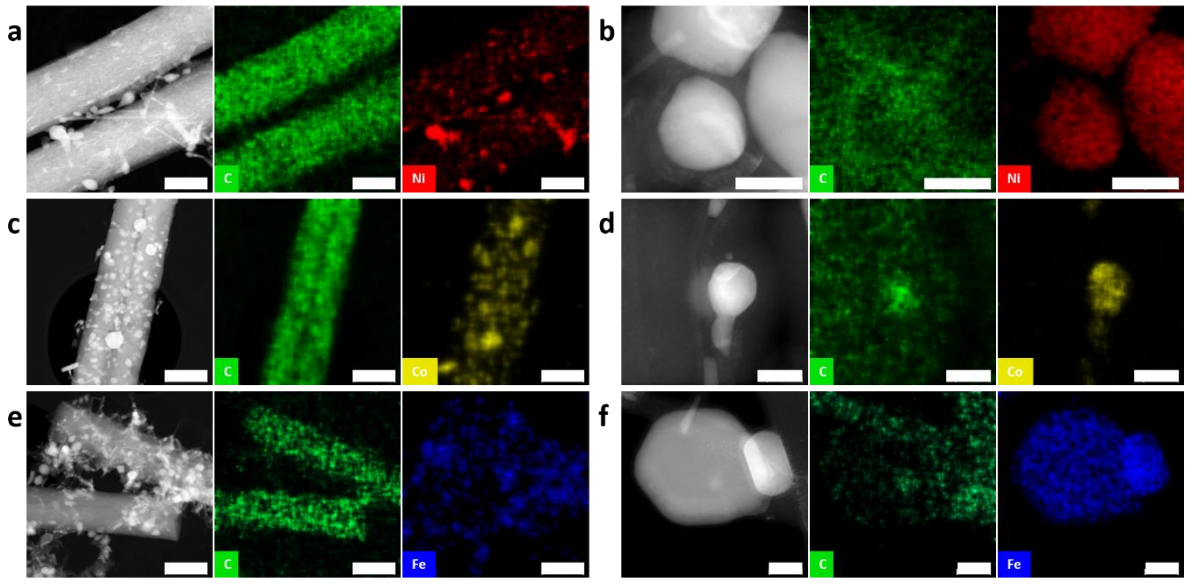

Fig. 3 | Elemental composition of the hairy fibres. a-f, STEM images for elemental mapping by energy-dispersive spectroscopy of Ni (a-b), Co (c-d) and Fe (e-f) based hairy carbon nanofibers. a,c,e, Lower magnification of larger carbon nanofiber covered with “hairs”. b,d,f, Magnified Ni, Co and Fe nanoparticles enclosed in nanotubes. (The scale bar is 400 nm and 40 nm in a,c,e and b,d,f, respectively.)

The X-ray diffraction (XRD) patterns obtained on these fabrics are presented in Supplementary Fig. S6 which further confirms the presence of carbon and the metallic phase in the CMFs across the varied mass ratios of precursors from 30% wt to 50 wt%. The (0 0 2) Bragg’s peak for carbon indicates the presence of

both graphite and amorphous carbon in all fibres which is line with the TEM measurements in Fig. 2 and Fig. 3. In both Supplementary Figs. S6a and S6b, the pure metallic phase of Ni and Co can be identified. In Supplementary Fig. S6c, the Bragg's peaks in the Fe fibres indicates the presence of phases other than pure Fe and C. On the Fe40 pattern (Fe40, post carbonised from electrospun nanofiber with 40 wt% $Fe(acac)_3$), Le Bail refinement was carried out using the P n m a(63) space group for Fe_3C cementite having an orthorhombic structure (Supplementary Fig. S6d). The Chi [27] for the Le Bail refinement was found to be 1.15 which suggests that the Fe and C have reacted to form cementite during the heat treatment. From the XRD patterns, the crystallite sizes for the metallic phases were found to be approximately 20 nm, which is in line with TEM measurements. The calculations based on the C (0 0 2) peak position for the Co and Ni fibres show the highest degree of graphitisation, whilst this could not be accurately calculated for the Fe fibres due to overlapping of the Fe_3C peaks and C (0 0 2) in the XRD patterns. In both the Ni and Co fibres, the samples with 40% metal loading showed the highest degree of graphitisation (Supplementary Table S2). A detailed XPS analysis performed on these samples confirms the metallic nature of the nanoparticles and graphitic carbon with pyridine Nitrogen (Supplementary Fig. S7)

Growth Mechanism of the CMFs. In the pre-carbonisation process, metal oxide nanoparticles are formed in the nanofibers from the metal salt additives, which are then reduced to form metal domains upon further heat treatment. These nanoparticles diffuse to the surface of the CNFs through an exsolution mechanism resulting in a nanoparticle decorated CNF. Given that the subsequent carbonisation was carried out under a N_2 atmosphere with no additional carbon source present, it is proposed that the feedstock for growth of the CNT "bristles" were the by-products of the thermal decomposition of PAN, which includes carbon species such as CH_4 and CO[28]. These gases are decomposed *in-situ* leading to the deposition of carbon at the nanoparticle surface, leading to the formation and growth of the CNT "bristles". Fig. 4 shows the proposed route for the growth of carbon nanotubes on electrospun fibres leading to CMFs, which is in line with control experiments performed at lower temperatures.

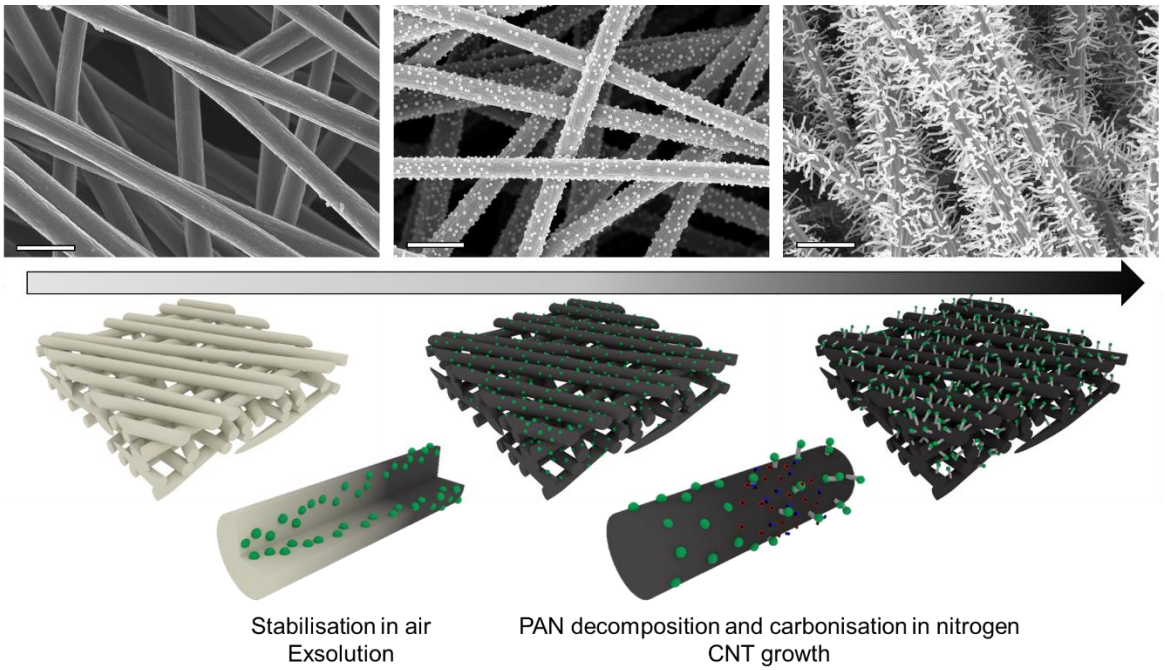

Fig. 4 | SEM and diagrammatic representation images of the various stages of synthesis for the CMFs. Light fibres represent uncarbonised PAN, green particles are catalyst particles and dark fibres are stabilised and carbonised fibres. Scale bar = 2 μm.

For example, the SEM images of the surface morphology of the Fe based electrospun nanofibers with different heat treatment stages are shown in Supplementary Fig. S1. Compared to electrospun fibres before carbonisation, small nanoparticles are formed after pre-carbonisation, where these small nanoparticles tend to form larger nanoparticles at higher temperatures of 550 °C, with the "bristle" found with further heat treatment to 850 °C. The same trends can also be found in Co and Ni based carbon nanofibers (Supplementary Figs. S2 and S3). As evidenced in the TGA results (Supplementary Fig. S8), the slight mass decrease of the metal salt precursors at temperatures below 200 °C was due to the loss of absorbed free water and bound water. The thermal decomposition after 200 °C was rapid, resulting in a dark precipitate. According to the literature[29], nanoscale Fe, Co and Ni oxides (Fe_3O_4, CoO and NiO) can be obtained. Therefore, nano-dimensional metal oxides can be obtained by the decomposition of their metal salt precursors during the stabilization of the electrospun nanofibers. This reaction is terminated after 400°C, but a pre-carbonisation temperature of 290 °C was selected for the consideration of good stabilisation of the PAN. The Raman spectra of the as-prepared materials is characterised by two main bands; the graphitic (G) band, which occurs at ~1,600 cm^{-1}; and the disordered (D) band, which occurs ~1,350 cm^{-1}. As shown in Supplementary Fig. S9, the PAN

powder does not show D and G bands while the electrospun PAN fibres show intense D and G bands characteristic of highly ordered material. When the electrospun fibres are doped with $Fe(acac)_3$, $Co(acac)_2$, and $Ni(acac)_2$, the resulting nanofibers shift the D and G bands to higher wavenumbers. The shift of the D and G bands can be attributed to the formation of metal oxides on fibers after pre-carbonisation treatment (Fe/Co/Ni_after PT). During the carbonization of the PAN, H_2 is released which can reduce the metal oxides present to form metal nanoparticles. Meanwhile, CH_4 and CO are released during decomposition of PAN above 400 °C and these gases are dissociated at the surface of the metal catalytic domains, followed by carbon precipitation (via surface or volumetric diffusion) to initiate the CNT growth[30]. As seen from the SEM images (Supplementary Figs. S1e, S1f, S2e S2f, S3e and S3f), the size of the Ni nanoparticles are larger than their Fe and Co based counterparts, resulting in the larger diameter of the grown CNT "bristle". This can be shown by the SEM images of the as-prepared carbon nanofibers (Supplementary Figs. S1g, S1h, S2g, S2h, S3g and S3h), where the Ni based CMF have largest diameter "bristles".

Apart from the typical base- and tip- growth mode of CNTs, these structures also exhibit mixed-growth mechanisms that lead to peapod like carbon nanotubes with multiple metal domains. We therefore calculated the binding energies between different metal clusters and the CNT to further understand the CNT growth on the electrospun fibres. Here, the binding energies of Ni, Co and Fe clusters on CNTs were found to be -3.84 eV, -2.75 eV and -2.84 eV, respectively (Supplementary Fig. S10). CNT growth may shift from base-growth to tip-growth with decreasing binding energy, indicating that Ni should show the strongest base growth mechanism while Co will experience more tip growth. This is experimentally confirmed from SEM images of their structures (Supplementary Figs. S4 and S5). Interestingly, the unique peapod like carbon nanotubes as shown in Supplementary Figs. S4b and S5b deviate from the above growth types. The mixed growth routes observed here can be attributed to use of carbon based substrates, which is conducive to metal diffusion (and floating catalyst). Compared to modelling results based on a Si substrate (Supplementary Fig. S11), the binding energies of Ni, Co and Fe clusters on carbon based substrate are much smaller than those for the Si (111) surface[31] (-21.88 eV for Ni, -16.16 eV for Co, -13.24 eV for Fe). This weaker binding

energy for Ni, Co and Fe on carbon indicates and the possibility of mixed growth mechanisms for all three carbon based materials, thus allowing the formation of the peapod structures. As can be seen in Supplementary Fig. S5b, the CNT "bristles" formed via each different growth mechanism can be found in the same backbone fibre, where the tip- and base-growth can be seen together with peapod structures. More base-grown CNTs are found on Ni based fibers, as illustrated in Supplementary Fig. S3h and as a result more peapod structures can also be found in Ni based fibers (Supplementary Fig. S4).

Furthermore, density functional theory (DFT) calculations shows that the binding energies between the (111) surfaces of the Fe, Ni and Co with C6 were found to be -9.46 eV, -7.59 eV and -7.32 eV respectively (Supplementary Table S3). This trend in binding energies between the metal domain and the carbon matches with observations in the thicknesses of carbon coatings on the nanoparticles. In the case of the Fe which has the strongest binding energy with the carbon, the thinnest carbon coating is observed. This suggests that once the first few layers of carbon are formed on the Fe it becomes difficult for additional carbon layers to be grown under this due to strong stabilisation (high binding energy) leading to difficulty in lifting the previous carbon layer up resulting in a relatively thin coating. In the case of the Ni and Co, which have similar binding energies, the thickness of the carbon coating is similar. Since the binding energy is lower than that of Fe, the growth of the carbon layers thus becomes easier as the initially formed carbon layer is more weakly bound. In addition, Jingde et al [32] demonstrated that the energy barrier for carbon surface diffusion and carbon nucleation on the metals follows the order: Ni $\approx$ Co < Fe, suggesting that carbon can diffuse and nucleate easily on surface of Ni and Co, which further indicates formation of a thicker carbon coating on their surface. In the TEM results, this thicker carbon layer thus results in a more graphitic domain close to the metal domain but a more amorphous region further from the metal domain which is likely due to stretching of the outer carbon layers during the coating growth leading to distortion of the graphitic domains.

All solid state Zn-air batteries via carbon metal fabrics. To demonstrate the potential of CMFs in electrochemical energy storage devices, we have designed and fabricated all-solid-state rechargeable zinc-air batteries. All of the batteries are composed of a zinc metal foil anode, a PAN:poly(ethylene

oxide) (PAN:PEO, 4:6) hydrogel electrolyte (Supplementary Fig. S12), a pressed nickel foam current collector, and the free-standing CMF as the air cathodes. Fig. 5b shows the polarization and power density curves of the Fe (40%) based CMFs (with "bristles") and metal CMFs (without "bristles") having the same mass loading of Fe, and CNF without any Fe.

The CMFs with CNT bristles offer a 113% increase in power density when compared to the non-hairy Fe-added CNF, and a 297% increase when compared to the CNF with no Fe. This observation, together with morphology and structural characterisation is attributed to the CMF with bristles enhancing the nanoporous 3D carbon network by increasing the specific surface area, number of electron pathways and also providing a catalytic domain for oxygen evolution/reduction. Additionally, the metal CNF electrodes maintain a high open circuit voltage (OCV) of 1.25 V but can reach up to 1.45 V when CMFs are used (Supplementary Fig. S13, picture of the OCV of 1.45 V for single cell and 2.99 V for two cells connected in series). Furthermore, these fabrics exhibit a lower charge-discharge voltage gap than that of the metal CNF, indicating the better rechargeability of the zinc-air batteries with CMFs as air cathode (Fig. 5a).

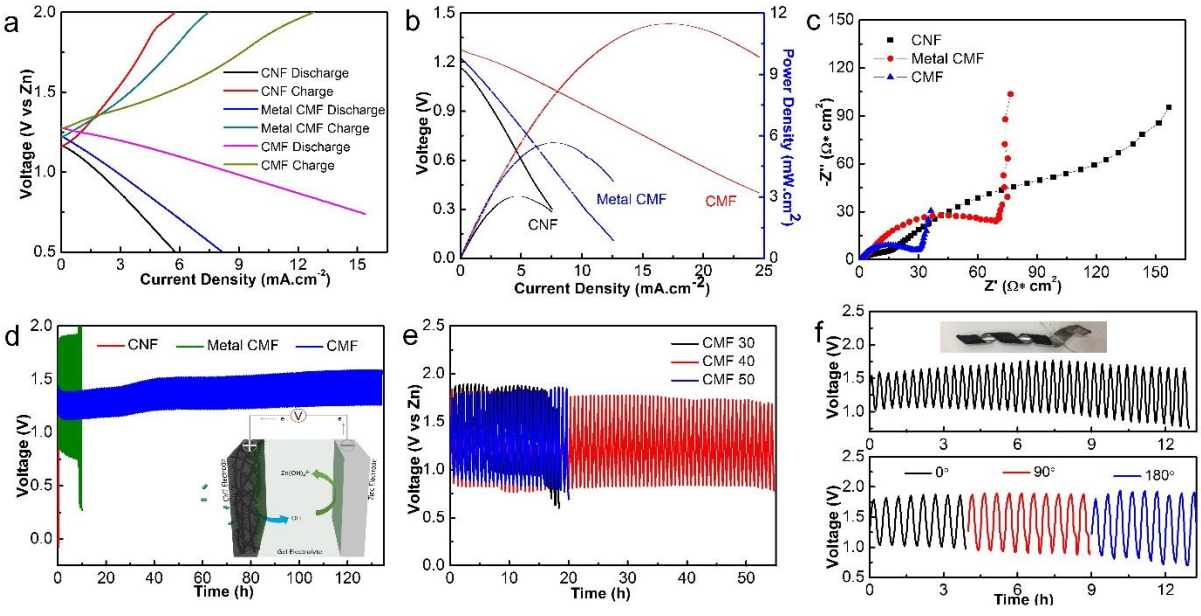

Fig. 5 | Fe based CMF applied for Zn-air battery. a, Charge and discharge polarization curves of all-solid-state rechargeable zinc-air batteries with different air cathodes. b, Polarization and power density curves of all-solid-state rechargeable zinc-air batteries with different air cathodes. c, Nyquist plots of the impedance of the all-solid-state rechargeable zinc-air batteries in the frequency range of 500 kHz to 0.05 Hz. d, Galvanostatic discharge-charge cycling curves at 0.5 mA cm^{-2} for the all-solid-state rechargeable zinc-air batteries for different air

cathodes (insert schematic of Zn-Air battery with CMFs). e, Galvanostatic discharge-charge cycling curves at 0.5 mA cm^{-2} for the all-solid-state rechargeable zinc-air batteries for different air cathodes with different Fe concentration. f, Flexible and twistable all-solid-state rechargeable zinc-air battery.

Furthermore, in assessing the electrochemical impedance spectra (EIS) for the different air cathodes, the Nyquist plots indicate a smaller charge transfer resistance for the CMFs in comparison to the other materials (Fig. 5c). These electrochemical enhancements demonstrate the advantage of CMFs with fine CNT "bristles", which can increase the surface area, facilitate the 3D porous fibre network and do not block the oxygen diffusion pathways across electrodes. Galvanostatic discharge-charge cycling curves for the flexible all-solid-state rechargeable zinc-air batteries at 0.5 mA cm^{-2} are then demonstrated with twisted electrodes and different curvatures of 0°, 90°, and 180° (Fig. 5f). Along with its high flexibility and better electrochemical performance compared to the metal CNFs, our CMF fabrics also offer a significant improvement in cycle life due to their favourable bifunctional catalytic properties and increased specific surface area. Fig. 5d demonstrates the stable galvanostatic cycling performance of the Fe based fabrics (10 min charge and 10 min discharge for each cycle), which outperform the metal CNF electrodes at the current density of 0.5 mA cm^{-2}. SEM analysis of the CMF electrodes after one cycle and 135 hours charge/discharge cycles are shown in the Supplementary Fig. S14, where the deposition of discharge products are found to be well confined within these fabrics and the battery failure is be mainly attributed to the electrolyte evaporation. In this regard, Supplementary Fig. S15 shows the atomic Hirshfeld charge distribution of a Fe atom inside the CNT, which highlights the ability of this material to help delocalize the charge distribution. The concentration of the Fe catalytic domains in the fabrics can also be directly controlled to 30%, 40% and 50% as shown in Fig. 5e where the Fe40 CMFs achieve the best cycling stability for nearly 60 hours of cycling a current density of 0.5 mA cm^{-2} (15 min charge and 15 min discharge for each cycle). The assembled Zn-air batteries also show good performance even when the battery is twisted into a spiral shape (Fig. 5f) and can be operated under different bending conditions without compromising on their electrochemical performance (Supplementary Fig. 16). Compared to the recently reported all-

solid-state Zn-air batteries (Supplementary Table S3), CMFs based Zn-air battery can achieve comparable electrochemical performance, while being fully mechanically flexible.

Conclusion

A tractable route to manufacture non-woven carbon fabrics made up of electrospun carbon fibres bearing carbon nanotube bristles that contain catalytically active metal nanoparticles has been presented. Our microscopic, spectroscopic and modelling has shown that these self-assembling hierarchical structures come about through the decomposition and exsolution of low-cost acetylacetonate salts of Ni, Co and Fe which form surface nanoparticles on electrospun and heat treated PAN fibres in air. Further, carbonisation results in CNT "bristle" growth in N_2 where the carbon source is provided by the decomposition products of the PAN resulting in CMFs which have a combination of base-growth, tip-growth and peapod like structures due to the low binding energy of the metal to the CNF. The metallic domains are all coated in a carbon layer which is found to have a graphitic core region and disordered shell region. These free standing, mechanically flexible and twistable fabrics can be used as electrodes for next generation energy storage devices. As a proof of concept, these CMFs were utilized as air cathodes in an all-solid-state Zn air battery, resulting in double the power density when benchmarked against plain carbon fibres.

Emails of corresponding authors:

*panfeng@pkusz.edu.cn; *chandramohan.george@imperial.ac.uk, *billy.wu@imperial.ac.uk

Acknowledgements

This work was kindly supported by the EPSRC energy storage for low carbon grids project (EP/K002252/1), the EPSRC Joint UK-India Clean Energy Centre (JUICE) (EP/P003605/1), the EPSRC Multi-Scale Modelling project (EP/S003053/1), and the Innovate UK for Advanced Battery Lifetime Extension (ABLE) project, Soft Science Research Project of Guangdong Province (No. 2017B030301013), Shenzhen Science and Technology Research Grant (ZDSYS201707281026184). Swansea University College of Engineering Advanced Imaging of Materials (AIM) Facility, which was funded by the EPSRC (EP/M028267/1), the European Regional Development Fund through the Welsh Government (80708), and the Ser Solar project via Welsh Government. CG acknowledges The Royal Society for an URF.

+ These authors contribute equally to this work.

References

1. Dai, L., Chang, D. W., Baek, J. B. & Lu, W. Carbon nanomaterials for advanced energy conversion and storage. *Small* (2012). doi:10.1002/smll.201101594

2. Candelaria, S. L. *et al.* Nanostructured carbon for energy storage and conversion. *Nano Energy* (2012). doi:10.1016/j.nanoen.2011.11.006

3. S. Iijima, Nature 354 (1991) 56..pdf. doi:10.0.4.14/354056a0

4. Landi, B. J., Ganter, M. J., Cress, C. D., DiLeo, R. A. & Raffaelle, R. P. Carbon nanotubes for lithium ion batteries. *Energy Environ. Sci.* (2009). doi:10.1039/b904116h

5. Wu, S. *et al.* Graphene-Containing Nanomaterials for Lithium-Ion Batteries. *Advanced Energy Materials* (2015). doi:10.1002/aenm.201500400

6. Zhang, J., Xia, Z. & Dai, L. Carbon-based electrocatalysts for advanced energy conversion and storage. *Sci. Adv.* (2015). doi:10.1126/sciadv.1500564

7. Lightcap, I. V. & Kamat, P. V. Graphitic design: Prospects of graphene-based nanocomposites for solar energy conversion, storage, and sensing. *Acc. Chem. Res.* (2013). doi:10.1021/ar300248f

8. Li, X., Chen, Y., Huang, H., Mai, Y. W. & Zhou, L. Electrospun carbon-based nanostructured electrodes for advanced energy storage - A review. *Energy Storage Materials* (2016). doi:10.1016/j.ensm.2016.06.002

9. Wang, C. *et al.* Proton Exchange Membrane Fuel Cells with Carbon Nanotube Based Electrodes. *Nano Lett.* (2004). doi:10.1021/nl034952p

10. Li, W. *et al.* A self-template strategy for the synthesis of mesoporous carbon nanofibers as advanced supercapacitor electrodes. *Adv. Energy Mater.* (2011). doi:10.1002/aenm.201000096

11. Li, Z., Zhang, J. T., Chen, Y. M., Li, J. & Lou, X. W. Pie-like electrode design for high-energy

density lithium-sulfur batteries. *Nat. Commun.* (2015). doi:10.1038/ncomms9850

12. Zhang, B., Kang, F., Tarascon, J. M. & Kim, J. K. Recent advances in electrospun carbon nanofibers and their application in electrochemical energy storage. *Progress in Materials Science* (2016). doi:10.1016/j.pmatsci.2015.08.002

13. Cavaliere, S., Subianto, S., Savych, I., Jones, D. J. & Rozière, J. Electrospinning: Designed architectures for energy conversion and storage devices. *Energy and Environmental Science* (2011). doi:10.1039/c1ee02201f

14. Wang, H. G., Yuan, S., Ma, D. L., Zhang, X. B. & Yan, J. M. Electrospun materials for lithium and sodium rechargeable batteries: From structure evolution to electrochemical performance. *Energy and Environmental Science* (2015). doi:10.1039/c4ee03912b

15. Liu, X. *et al.* Flexible all-fiber electrospun supercapacitor. *J. Power Sources* **384,** (2018).

16. Liu, K. *et al.* Electrospun core-shell microfiber separator with thermal-triggered flame-retardant properties for lithium-ion batteries. *Sci. Adv.* (2017). doi:10.1126/sciadv.1601978

17. Zhu, C., Yu, Y., Gu, L., Weichert, K. & Maier, J. Electrospinning of highly electroactive carbon-coated single-crystalline LiFePO4 nanowires. *Angew. Chemie - Int. Ed.* (2011). doi:10.1002/anie.201005428

18. Xiong, X. *et al.* Flexible membranes of MoS2/C nanofibers by electrospinning as binder-free anodes for high-performance sodium-ion batteries. *Sci. Rep.* (2015). doi:10.1038/srep09254

19. Liu, Q., Wang, Y., Dai, L. & Yao, J. Scalable Fabrication of Nanoporous Carbon Fiber Films as Bifunctional Catalytic Electrodes for Flexible Zn-Air Batteries. *Adv. Mater.* **28,** 3000–3006 (2016).

20. Jung, K. N. *et al.* One-dimensional manganese-cobalt oxide nanofibres as bi-functional cathode catalysts for rechargeable metal-air batteries. *Sci. Rep.* (2015). doi:10.1038/srep07665

21. Iqbal, N. *et al.* Flexible Fe3O4@carbon nanofibers hierarchically assembled with MnO2 particles for high-performance supercapacitor electrodes. *Sci. Rep.* (2017).

doi:10.1038/s41598-017-15535-x

22. Radacsi, N., Campos, F. D., Chisholm, C. R. I. & Giapis, K. P. Spontaneous formation of nanoparticles on electrospun nanofibres. *Nat. Commun.* (2018). doi:10.1038/s41467-018-07243-5

23. Liu, Y. *et al.* Hierarchical porous carbon fibers/carbon nanofibers monolith from electrospinning/CVD processes as a high effective surface area support platform. *J. Mater. Chem. A* **5,** 2151–2162 (2017).

24. Zhang, S. *et al.* Direct electronetting of high-performance membranes based on self-assembled 2D nanoarchitectured networks. *Nat. Commun.* (2019). doi:10.1038/s41467-019-09444-y

25. Lai, C., Guo, Q., Wu, X. F., Reneker, D. H. & Hou, H. Growth of carbon nanostructures on carbonized electrospun nanofibers with palladium nanoparticles. *Nanotechnology* **19,** (2008).

26. Yao, Y. *et al.* Carbothermal shock synthesis of high-entropy-alloy nanoparticles. *Science (80-.).* **359,** 1489–1494 (2018).

27. Maire, J. & Mering, J. Graphitization of Soft Carbons. *Chem. Phys. Soft Carbons* **6,** 125–190 (1970).

28. Donnet, J. & Bahl, O. *Encyclopedia of Physical Science and Technology*. (New York: Acedamic Press Inc., 1987).

29. Li, Y., Afzaal, M. & O'Brien, P. The synthesis of amine-capped magnetic (Fe, Mn, Co, Ni) oxide nanocrystals and their surface modification for aqueous dispersibility. *J. Mater. Chem.* **16,** 2175–2180 (2006).

30. Rahaman, M. S. A., Ismail, A. F. & Mustafa, A. A review of heat treatment on polyacrylonitrile fiber. *Polym. Degrad. Stab.* **92,** 1421–1432 (2007).

31. Kordás, K., Pap, A. E., Vähäkangas, J., Uusimäki, A. & Leppävuori, S. Carbon nanotube synthesis on oxidized porous silicon. *Appl. Surf. Sci.* **252,** 1471–1475 (2005).

32. Li, J., Croiset, E. & Ricardez-Sandoval, L. Carbon nanotube growth: First-principles-based kinetic Monte Carlo model. *J. Catal.* **326,** 15–25 (2015).

Extended information

CMFs production: The precursor solution was first prepared by mixing 0.8 g Iron (III) acetylacetonate $Fe(acac)_3$ and 12 ml DMF (Fig. 1a upper photo), followed by adding 1.2 g of PAN, whereby a dark orange solution was obtained after magnetic stirring the mixture at 55 °C for 24 h (Fig. 1a lower photo). For the electrospinning process, the as-prepared precursor solution was transferred to a syringe and driven into the electrospinning needle at 1.5 ml/h by a syringe pump. The needle (19 G, double) was held at 13 kV provided by a high voltage power supply (GenVolt 73030), with a working distance of 20 cm from the grounded rotating collector (rotating speed 2,000 RPM, 25 °C, 50% humidity). An orange coloured electrospun nanofiber film is produced via this process, as shown in Fig. 1a. Following the same preparation process, Cobalt (II) acetylacetonate (Co(acac)2) and Nickel (II) acetylacetonate $Ni(acac)_2$ were also used to create nanofiber films. Their mixtures with DMF (Figs. 1b and 1c, upper) and DMF+PAN (Figs. 1b and 1c, lower) were electrospun resulting in pink coloured $Co(acac)^2$ doped PAN nanofibers and green colour $Ni(acac)_2$ doped PAN nanofiber films.

The as-prepared nanofibres were peeled off the aluminium foil attached to the rotating collector and the Fe/Co/Ni based nanofiber films were stabilized at 290 °C in air for 2 h with a ramp rate of 2 °C min^{-1}. Then the films were fully carbonised at 850 °C in N_2 (initial ramp rate of 2 °C min^{-1}, dwell time of 2 h at 300 °C, ramp rate of 5 °C min^{-1} to 850 °C, dwell time 2 h). On completion of the heat treatment, growth of carbon nano-hairs with metallic catalytic domains on the electrospun fabrics were achieved. SEM images are shown in Figs. 1d and 1g for Fe based fabric, Figs. 1e and 1h for Co based fabrics, and Figs. 1f and 1i for Ni based HCNF show the hierarchical micro/nanostructure which resembling fine bristles found in certain plants and insects. These Fe, Co and Ni based nanotubes have diameters approximately of 10-50 nm and up to several hundred nanometers (approximately 600 nm) in length. Compared to other preparation methods (Supplementary Table S1), our CMF can be

obtained, via a facile preparation method without catalyst deposition, catalyst activation and without an additional carbon source being introduced.